PELDOR Measurements on a Nitroxide-Labeled Cu(II) Porphyrin: Orientation Selection, Spin-Density Distribution, and Conformational Flexibility

Bela E. Bode, Jörn Plackmeyer, Thomas F. Prisner, and Olav Schiemann*,†

Institute of Physical and Theoretical Chemistry and Center for Biomolecular Magnetic Resonance, Max-von-Laue-Strasse 7, J. W. Goethe-University, 60438 Frankfurt am Main, Germany

Received: October 31, 2007; Revised Manuscript Received: March 7, 2008

Metal ions are functionally or structurally important centers in metalloproteins or RNAs, which makes them interesting targets for spectroscopic investigations. In combination with site-directed spin labeling, pulsed electron−electron double resonance (PELDOR or DEER) could be a well-suited method to characterize and localize them. Here, we report on the synthesis, full characterization, and PELDOR study of a copper(II) porphyrin/nitroxide model system. The X-band PELDOR time traces contain besides the distance information a convolution of orientational selectivity, conformational flexibility, exchange coupling, and spin density distribution, which can be deconvoluted by experiments with different frequency offsets and simulations. The simulations are based on the known experimental and spin Hamiltonian parameters and make use of a geometric model as employed for structurally similar bis-nitroxides and spin density parameters as obtained from density functional theory calculations. It is found that orientation selection with respect to dipolar angles is only weakly resolvable at X-band frequencies due to the large nitrogen hyperfine coupling of the copper porphyrin. On the other hand, the PELDOR time traces reveal a much faster oscillation damping than observed for structurally similar bis-nitroxides, which is mainly assigned to a small distribution in exchange couplings *J*. Taking the effects of orientation selectivity, distribution in *J*, and spin density distribution into account leads finally to a narrow distance distribution caused solely by the flexibility of the structure, which is in agreement with distributions from known bis-nitroxides of similar structure. Thus, X-band PELDOR measurements at different frequency offsets in combination with explicit time trace simulations allow for distinguishing between structural models and quantitative interpretation of copper-nitroxide PELDOR data gives access to localization of copper(II) ions.

Introduction

Metal ions are crucial for the structure and function of catalytically active metalloproteins[1] and RNAs.[2] To characterize the role of individual metal ions, biophysical methods probing the local structure of these ions and their position within the global fold of the biopolymer in solution are needed. Nuclear magnetic resonance (NMR) spectroscopy is frequently applied for such purposes, but reaches its limits in cases of large biomacromolecular complexes or in the case of paramagnetic metal centers like copper(II), manganese(II), molybdenum(V), or iron(III).[3] However, paramagnetic centers or the exchange of diamagnetic ions by paramagnetic ones enables the application of continuous wave (CW) and pulsed electron paramagnetic resonance (EPR) techniques,[4] which were proven to yield detailed and precise information about local structures of metal ion binding pockets in proteins[5] and RNAs.[6] EPR methods have also been shown to yield reliable results with respect to locating ions in relation to other metal centers or organic cofactors.[7] In a similar approach, paramagnetic metal ions may also be localized via distance measurements to artificially and site-directedly attached nitroxides; attempts based on relaxation measurements have been reported.[8] A pulsed EPR method that has been demonstrated to be suitable and straightforward for measuring nanometer distances between nitroxides,[9] metal centers[10] and paramagnetic organic cofactors,[11] while exceeding the CW EPR limit (<2 nm) by up to 6 nm, is called pulsed electron−electron double resonance (PELDOR or DEER).[12] Another method for measuring dipolar couplings, which is less frequently applied, is double quantum coherence (DQC) EPR.[13] Yet, PELDOR distance measurements between a copper(II) ion and a nitroxide have only been reported once for an in situ generated model compound;[14] that PELDOR measurements involving Cu^{2+} are feasible has been shown in three reports concerning copper−copper distances.[15] Nonetheless, general questions remain with respect to the influence of orientation selection,[15c,16] conformational flexibility,[15c,17] and spin density distribution.[10b,c]

Here, we introduce a newly synthesized and fully characterized asymmetric copper(II)porphyrin-nitroxide model system and show that a detailed analysis of the PELDOR time domain data yields, even in the presence of strong spin delocalization, the precise copper-nitroxide distance and the conformational flexibility of the molecule. In addition, we discuss the influence of orientation selection and exchange coupling based on simulations of the experimental data.

Methods and Materials

Synthesis. All reactions were performed with exclusion of air under argon employing standard Schlenk techniques. Reagent-grade solvents and chemicals were used without further purification, except where stated otherwise. Dry solvents were purchased from Fluka or ACROS and thoroughly degassed prior

* To whom correspondence should be addressed. E-mail: os11@st-andrews.ac.uk.

† Current address: Center of Biomolecular Science, School of Biology, University of St. Andrews, St. Andrews, Fife, KY16 9UA, Scotland.

10.1021/jp710504k CCC: $40.75
Published on Web 05/20/2008

to use. Triethylamine was freshly distilled from CaH_2. Solvents and reagents for Sonogashira cross-couplings were degassed by freeze−pump−thaw cycles. Octaethylporphyrin (H_2(OEP)) and copper(II)-octaethylporphyrin (Cu(OEP)) were purchased from Aldrich and 4-hydroxy-4′-iodobiphenyl from ABCR. 1-Oxyl-2,2,5,5-tetramethylpyrrolin-3-carboxylic acid (TPC) **1** was prepared from 2,2,6,6-tetramethyl-4-oxopiperidine by modified procedures of Hideg et al.[18] TLC: SiO_2 60 F_{254} and Al_2O_3 60 F_{254} neutral both from Merck. Column chromatography: SiO_2 60 (70−230 mesh) from Aldrich or Al_2O_3 MP Alumina N−Super I from MP Biomedicals.

Analytic observations relied on elemental analysis and mass spectrometry such as electron ionization (EI), electrospray ionization (ESI), and MALDI. EI mass spectra were recorded on a CH7A spectrometer from MAT, ESI mass spectra were recorded on a LCQ Classic spectrometer from Thermo Electron, and MALDI mass spectra were recorded on a Voyager DE-Pro or STR spectrometer, both from Applied Biosystems. Proton NMR spectra were acquired of diamagnetic molecules at 250 MHz on a Bruker AM-250 spectrometer and calibrated using residual nondeuterated solvents as internal standard (δ $CHCl_3$ = 7.240). Elementary analysis was performed on a Foss-Heraeus CHN-O-Rapid, and UV−vis spectra were recorded on an Agilent 8453 Spectrophotometer. Graphical representations of the crystal structure were produced using the WinGX software.[19]

The Ni(OEP)[20] and Ni(meso-formyl-OEP) derivatives of H_2(OEP) were prepared according to literature procedures.[21] Ni(meso-ethynyl-OEP) and Cu(meso-ethynyl-OEP) **2** were prepared according to ref 22 from a mixture of the corresponding meso-E/Z-2-chloroethenyl-OEP-compounds instead of the bromoethenyl derivatives (see Supporting Information) and used as obtained due to the products susceptibility to spontaneous oxidative dimerization.[23]

(1-Oxyl-2,2,5,5-tetramethyl-pyrrolin-3-carboxylic acid 4′-iodobiphenyl-4-yl-ester) (3). 1,3-dicyclohexylcarbodiimide (DCC) (1.671 g, 8.09 mmol) was added in one portion to a solution of TPC **1** (746 mg, 4.05 mmol), dimethylaminopyridine (DMAP) (900 mg, 8.10 mmol), and 4-hydroxy-4′-iodobiphenyl (800 mg, 2.70 mmol) in 20 mL of dry tetrahydrofuran (THF). After a yellow precipitate had formed, 10–12 mL of dry THF was added to facilitate stirring. The reaction was allowed to continue at room temperature over 3 d in the dark. All solids were removed by filtration and washed with a small amount of THF and then thoroughly washed with diethyl ether (150 mL). The yellow filtrate was evaporated to dryness, and the residue redissolved in diethyl ether. The ether solution was extracted with water and brine. After drying over sodium sulfate, the diethyl ether was removed and the yellow residue redissolved in diethyl ether/hexane 2:1 and was subjected to column chromatography (Al_2O_3, 4% H_2O, 4 × 18 cm). A bright yellow fraction was eluted first, directly followed by the broad yellow main band of the product. After removal of the solvent, a yellow solid was obtained (1.004 g, 2.17 mmol, 80%). Anal. Calcd for $C_{21}H_{21}INO_3$: C, 54.56; H, 4.58; N, 3.03. Found: C, 54.61; H, 4.63; N, 2.87. ESI-MS (+) *m*/*z* calcd for $C_{21}H_{21}INO_3$, 462.3; found, 462.8 (M^+, 100%).

(Cu(OEP)-TPC-ester) (4). To a solution of **3** (55 mg, 0.12 mmol) and $PdCl_2(PPh_3)_2$ (12.6 mg, 0.018 mmol) in 9 mL of NEt_3 and 5 mL of THF was added first CuI (12 mg, 0.06 mmol) and then a mixture of 74 mg (0.12 mmol) of Cu(meso-ethynyl-OEP) **2** and 12 mg (0.05 mmol) of PPh_3 in 4 mL of NEt_3 and 3 mL of THF. The resulting red-brown solution was stirred at room temperature for 16 h with exclusion of light and finally stirred at 50 °C for 1.5 h. After cooling to room temperature, the solvents were removed in vacuo, and the solid residue was redissolved in dichloromethane. The organic phase was washed three times with water and dried with sodium sulfate. After the solvent was removed in vacuo, the residue was redissolved in dicholoromethane/hexane (2:1) and purified via column chromatography (3 × 20 cm, Al_2O_3, 4% H_2O, dicholoromethane/hexanes (2:1)). A dark green band was eluted first, followed by a red-brown fraction containing unreacted **3** and the desired product. This main fraction was stripped from solvent, and the residue was recrystallized from chloroform layered with methanol. The product was obtained as red-violet leaflets and needles after filtration, washing with methanol, and drying in vacuo. Yield: 35 mg (0.037 mmol, 31%). Single crystals suitable for X-ray diffraction were obtained from a benzene solution layered with petroleum ether. Anal. Calcd for $C_{59}H_{64}N_5O_3Cu$: C, 74.22; H, 6.76; N, 7.34. Found: C, 74.07; H, 6.64; N, 7.28. UV−vis (benzene) λ_{max} (log ε): 426 nm (5.448), 554 (4.289), 594 (4.284). MALDI-TOF-MS (matrix, DHB) *m*/*z* calcd for $C_{59}H_{64}N_5O_3Cu$: 954.735. Found: 954.9 (M^+, 100%), 894.0 ($(M - 4 \times CH_3)^+$, 33%).

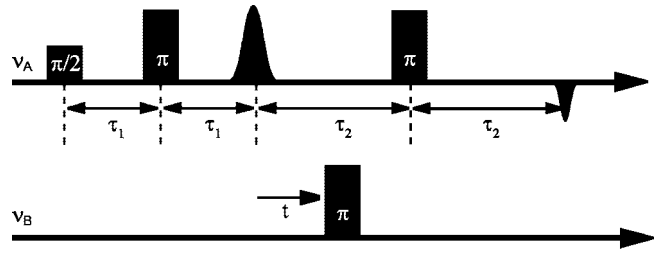

Figure 1. Pulse sequences for 4-pulse PELDOR.

PELDOR Theory. All following PELDOR experiments were performed with the 4-pulse sequence shown in Figure 1.

The pulses at the detection frequency ν_A create an echo from the spins on resonance, named in the following A spins (the unpaired electron centered at the Cu(II) porphyrin in this study). Introduction of an inversion pulse at the pump frequency ν_B flips spins resonant with this second frequency, here defined as B spins (here the electron spin centered at the nitroxide). The dipole−dipole splitting ω_{dd}, between A and B spins causes a shift in the Larmor frequency of the A spins by $\pm\omega_{dd}$. Therefore, after pumping the B spins the A spins accumulate a phase shift $\omega_{dd}t$, where t defines the time delay of the pump pulse. The resulting PELDOR signal $V(t)$ is a product of two contributions (eq 1)

$$V(t) = V_{intra}(t)V_{inter}(t) \quad (1)$$

$V_{intra}(t)$ describes the intramolecular contribution, whereas $V_{inter}(t)$ takes into account the signal decay caused by a distribution of spin centers in the sample. In case of a homogeneous distribution $V_{inter}(t)$ is a monoexponential decay.[24] For a single orientation (so) of the magnetic field B_0, the intramolecular contribution $V_{intra}(t)_{so}$ can be described by eq 2[17b]

$$V_{intra}(t)_{so} = V_0(1 - \lambda[1 - \cos(\omega_{dd}t)]) \quad (2)$$

In eq 2, it is assumed that the spin-orientations are not changed due to spin diffusion or spin-lattice relaxation and that the exchange coupling J is negligible versus ω_{dd}. V_0 is the A spin echo intensity at $t = 0$, and λ is the fraction of B spins, which are coupled to the detected A spin and inverted by the pump pulse. Both, V_0 and λ are dependent on the polar angles of the magnetic field vector φ and ϕ, and λ also depends on the set of Euler angles Ω describing the orientation of spin B in the axis system of spin A. In the point-dipole approximation

and for small g-anisotropies, such that the spin states are quantized parallel to the external field, and in the weak coupling regime, ω_{dd} is given by eq 3

$$\omega_{dd} = -\frac{\mu_0 \mu_B^2}{4\pi\hbar} \frac{g_A g_B}{|r_{AB}|^3}(3\cos^2\theta - 1) \quad (3)$$

In eq 3, g_A and g_B are the g-values of the spins A and B, respectively, $\hbar$ is the Planck constant divided by 2π, r_{AB} is the distance vector connecting the spins, θ is the angle between r_{AB} and the external magnetic field, and μ_0 is the vacuum permeability.

For disordered powder samples, the observed echo intensity is obtained by integration over all magnetic field orientations:

$$V_{intra}(t) = \int\int V_0(1 - \lambda[1 - \cos(\omega_{dd}t)])\sin(\phi)\mathrm{d}\phi\mathrm{d}\varphi \quad (4)$$

The relative orientation of spin A, spin B and the vector r_{AB} will all be random, if angular correlations can be neglected. In this case, the integration over the Euler angles effectively averages the magnetic field orientation dependence of the modulation depth parameter λ,[25] which then allows converting the double integration over different magnetic field orientations in eq 4 into an integration over all dipolar angles θ

$$V_{intra}(t) = V_0\left(1 - \lambda\left[1 - \int_0^{\pi/2} \cos(\omega_{dd}t)\sin\theta\mathrm{d}\theta\right]\right) \quad (5)$$

Within these boundaries, the coupling between spins can be deduced parameter-free from the time domain signal by division of $V(t)$ by $V_{inter}(t)$ and cosine Fourier transformation or inversion of time or frequency domain data to the distance domain. Because these inversions is generally ill-posed usually regularization methods are employed such as Tikhonov regularization.[26]

If angular correlations between the spins exist, this simplification is not valid.[12b,27] The pump efficiency λ will depend on the mutual orientation of the two radicals A and B. Additionally, the orientation selectivity of the excitation of spin A described by V_0 in combination with the orientation selectivity of the pump pulse will lead to a distribution function $P(\theta)$ of dipolar angles that differs from the $\sin(\theta)$ distribution of uncorrelated spin centers. The echo signal intensity $V_{intra}(t)$ for a given pump and probe frequency can in such general case be described by[12b,25]

$$V_{intra}(t) = V_0\left(1 - \left[\int_0^{\pi/2} P(\theta)[1 - \cos(\omega_{dd}t)]\mathrm{d}\theta\right]\right) \quad (6)$$

with

$$P(\theta) = \lambda(\theta)\sin\theta \quad (7)$$

In these cases data inversion based on eq 5 might lead to erroneous results and inversions based on eq 6 have not yet been reported. Spin centers exhibiting large g- or hyperfine anisotropies and thus broad spectra, such as copper, might pronounce this effect due to high spectral selectivity of the pulses. We have therefore chosen to simulate the experimental Cu^{2+}/nitroxide PELDOR time traces from a conformational ensemble of molecules created by a simple geometrical model.

In case of extensive spin density delocalization the point-dipole approximation breaks down, and the dipolar coupling has to be calculated treating all spin-bearing atoms. Each point-dipole is broken up into point charges to reflect the delocalization of the spins. In this model, elements of the interaction tensor are given by eq 8[28]

$$d_{ij} = -\frac{\mu_0 \mu_B^2}{4\pi\hbar} g_A g_B \sum_m \sum_n \rho_m \rho_n \frac{r_{mn}^2 \delta_{ij} - 3 r_{mni} r_{mnj}}{r_{mn}^5} \quad (8)$$

where δ_{ij} is the Kronecker delta, m and n are the spin bearing atoms at centers A and B, respectively, ρ is their respective spin density, r_{mn} is the respective interatomic distances, and r_{mni} and r_{mnj} are the i and j components of these interatomic distance vectors in the A spin molecular frame. The sums extend over all point-charges that constitute the interacting spins. In this logical extension of the point-dipole the g-tensors are still approximated to be isotropic.

PELDOR Simulations. Simulations were performed based on eqs 2–4 and 6, with detection and pumping efficiencies explicitly calculated for each orientation, each hyperfine state of the nitroxide nitrogen, and each hyperfine state of the copper nucleus. The nitrogen hyperfine coupling of the porphyrin ring was assumed to be isotropic.[29] The respective resonance positions are computed based on the g- and hyperfine tensors of the free nitroxide[30] and Cu(OEP)[29,31] and the experimental values for pulse lengths and microwave frequencies. A conformational ensemble typically containing 1000 different conformers was generated, each characterized by a distance vector r_{AB}, with polar angles (ψ, η) in the axis system of spin A and Euler angles Ω describing the mutual orientation of spin center B with respect to A. Full rotational freedom about the acetylene and ester linkers together with a single, harmonic backbone bending mode with a normal distribution of $\pm 15°$ (standard deviation) was assumed. For each of these conformers, the resonance positions of spins A and B were calculated for all orientations of the magnetic field vector B_0 in the molecular axis frame of spin A (typically 20 000 orientations). Hyperfine and g-tensor axes were considered to be collinear to the molecular axis system. The resonance frequencies of spin B can be calculated after describing hyperfine and g-tensor of spin B in the coordinate system of spin A. Additionally, an inhomogeneous line width has been taken into account by a Gaussian distribution to calculate the final resonance frequencies for spin A and B, respectively. Lorentzian excitation profiles were calculated from the experimental pulse lengths, which empirically describe the excitation profiles of rectangular pulses with a sinusoidal B_1 distribution over the cavity. This allows to calculate the excitation functions of spin A and B, V_0 and λ, and thereafter the dipolar distribution function $P(\theta)$ for each conformer. The dipolar coupling constant was computed for each orientation of the magnetic field according to eq 3, determining g_A and g_B for the given field orientation from the copper and nitroxide g-tensors respectively. If the field strength (B_1) of the detection and pump pulses (approximated via their pulse lengths t_{PA} and t_{PB}, respectively) is not much larger than the coupling strength, λ will become a function of ω_{dd}, which can be approximated by eq 9.[32]

$$\lambda(\omega_{dd}) = \lambda(\theta)\exp(-4\omega_{dd}^2 \cdot t_{PA}^2)\exp(-4\omega_{dd}^2 \cdot t_{PB}^2) \quad (9)$$

The final PELDOR signal for a given frequency offset $\Delta\nu_{AB}$ between detection and pumping frequency is the sum over all conformers and all magnetic field orientations (typically 1000 $\times$ 20 000).

Accounting for delocalization, the dipolar tensor was calculated according to eq 8, which was then multiplied with the dipole moments of the two spins. To take g-tensor anisotropy into account the dipole moments were calculated by multiplication of the respective g-tensors with the electron spin angular momentum using the high field approximation. The dipolar

coupling was then computed from this as the energy difference between the two manifolds of the B spin.

All simulations were performed with a home-written MATLAB® program. More details regarding the program and structure generation procedure are described elsewhere.[17b] Tikhonov regularizations were performed with the program of G. Jeschke[32] and an optimized regularization parameter of 1.

PELDOR Measurements. Samples of all three molecules, Cu(OEP), nitroxide **1** and biradical **4** were prepared as d_8-toluene (200 μM, 80 μL) solutions. Five equivalents of 1-methylimidazole were added to both Cu^{2+}-porphyrin samples to prevent aggregation. The samples were degassed by several freeze-pump cycles and frozen in liquid nitrogen prior to sealing the sample tube. All PELDOR spectra were recorded on a Bruker ELEXSYS E580 pulsed X-band EPR spectrometer with a standard flex line probe head housing a dielectric ring resonator (MD5 W1) equipped with a continuous flow helium cryostat (CF935) and temperature control system (ITC 502), both from Oxford instruments. The second microwave frequency was coupled into the microwave bridge by a commercially available setup (E580-400U) from Bruker. All pulses were amplified via a pulsed traveling wave tube (TWT) amplifier (117X) from Applied Systems Engineering. The resonator was over-coupled to a quality factor Q of about 50. PELDOR experiments were performed with the pulse sequence $\pi/2(\nu_A)$-τ_1-$\pi(\nu_A)$-$(\tau_1 + t)$-$\pi(\nu_B)$-$(\tau_2 - t)$-$\pi(\nu_A)$-τ_2-echo. The detection pulses (ν_A) were set to 32 ns for both π and $\pi/2$ pulses and applied at a frequency 226 MHz higher than the resonance frequency of the resonator. The amplitude was chosen to optimize the refocused echo. The $\pi/2$-pulse was phase-cycled to eliminate receiver offsets. To achieve a frequency offset ($\Delta\nu_{AB}$) of 226 MHz, the pump pulse (ν_B) was set to 12 ns at the resonance frequency of the resonator. For $\Delta\nu_{AB} = 603$ MHz, ν_B was set to a frequency of 377 MHz lower than the resonance frequency of the resonator and the pump pulse length was set to 32 ns. The field was adjusted in such a way that in either case the pump pulse is applied to the maximum of the nitroxide spectrum, where it selects the central $m_I = 0$ transition of A_{zz} together with the $m_I = 0, \pm 1$ transitions of A_{xx} and A_{yy}. The pulse amplitude was in both cases optimized to maximize inversion of a Hahn-echo at the pump frequency. All spectra were recorded at 20 K with an experiment repetition time of 3 ms, a video amplifier bandwidth of 25 MHz and an amplifier gain of 63 dB. τ_1 was set to 400 ns and τ_2 to 1200 ns. Usually 150 scans were accumulated with 180 data points and time increments Δt of 8 ns giving an approximate measurement time of 3.5 hours. Typically 500 scans were accumulated for spectra with $\Delta\nu_{AB} = 603$ MHz giving an approximate measurement time of 10 hours. Proton modulation was suppressed by addition of 8 spectra of variable τ_1 with a $\Delta\tau_1$ of 8 ns.[33] For comparison with simulations and data inversion the time traces were divided by a mono-exponential decay and normalized to the point $t = 0$.

Density Functional Theory (DFT) Calculations. The calculations for **1** and **2** were performed using unrestricted Kohn-Sham[34] DFT methods as implemented in GAUSSIAN 03[35] and TURBOMOLE.[36] All structure optimizations were carried out with TURBOMOLE employing Becke's exchange functional B[37] and Perdew's P86[38] correlation functional, together with the TZVP basis set[39] for all atoms and accelerated with the RI approximation using the standard TZVP auxiliary basis set from TURBOMOLE.[40] For the computation of the Mulliken spin-densities with GAUSSIAN 03, a combination was chosen of Becke's three-parameter hybrid exchange functional B3[41] together with the Perdew/Wang correlation functional PW91.[42]

SCHEME 1: Synthesis of Model Compound 4

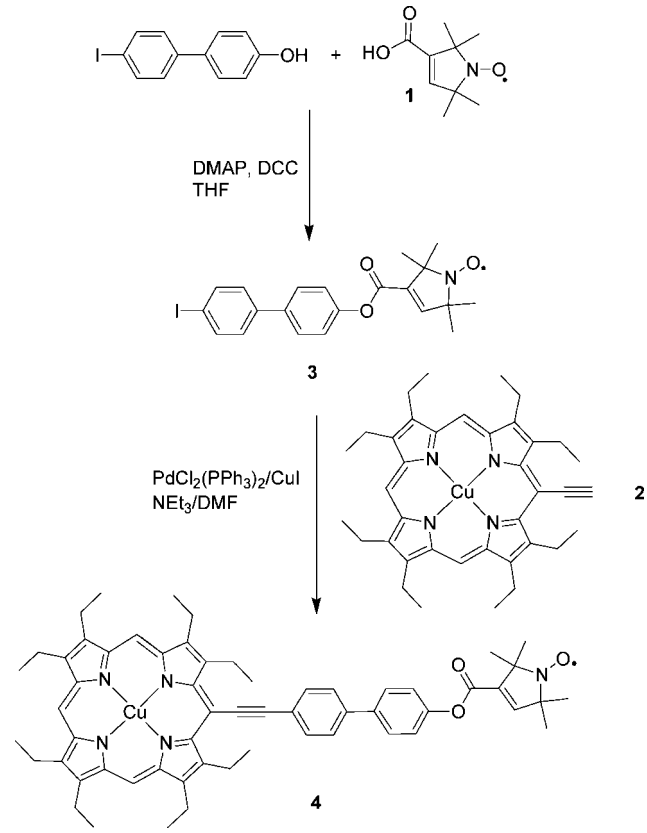

An ultrafine integration grid (58410 integration points per atom) and standard SCF=Tight convergence criteria were applied. For these calculations, a decontracted FII-A basis set of Arbuznikov et al.[43] (16s,13p,10d)/[11s,10p,10d] was used for Cu and the Huzinaga−Kutzelnigg-type IGLO-II basis sets[44] were used for all other atoms: (5s,1p)/[3s,1p] for H and (9s,5p,1d)/[5s,4p,1d] for C, O, and N.

Results and Discussion

Synthesis. Molecule **4** was chosen to be a suitable model system for studying the effects of spin delocalization, orientation selection and conformational flexibility on Cu^{2+}/nitroxide PELDOR measurements. The Cu(OEP) moiety resembles binding motives found in proteins, ensures considerable amount of spin density distribution into the coordinated ligand, and the interconnecting bridge allows for some degree of structural flexibility. In addition, the synthesis allowed for the covalent attachment of only one nitroxide group to the copper complex, in contrast to the previously reported in situ-synthesis of a copper-bis(terpyridyl) derivative.[14] The two step synthesis of the model compound is summarized in Scheme 1. In the initial step, the nitroxide-carboxylic acid **1** was coupled to the precursor bridge 4-hydroxy-4′-iodobiphenyl via esterification using DMAP and DCC as accelerators. In the second step, the resulting 4′-iodobiphenyl-ester **3** was attached to Cu(meso-ethynyl-OEP) **2** by means of Sonogashira cross-coupling yielding the desired nitroxide-metallo-porphyrine **4** in an overall yield of 33%.

X-ray Structure. Crystals of **4** suitable for X-ray diffraction could be grown from benzene.[45] A graphical representation of the molecular structure is shown in Figure 2 and selected bond lenghts and angles are given in tables S1 to S3 in the Supporting Information. The compound forms a triclinic crystalline system and exhibits significant deviations of the porphyrinic ring from

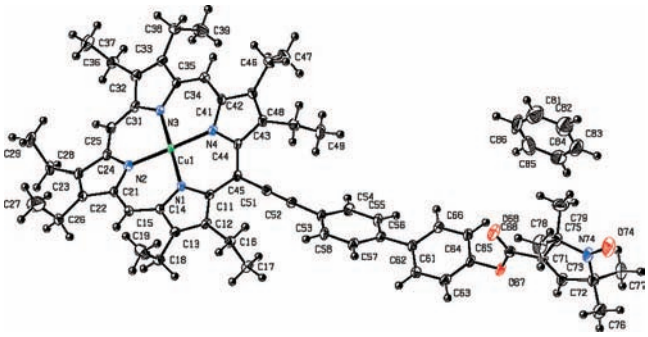

Figure 2. Molecular structure of the nitroxide substituted Cu^{2+}-porphyrin **4**.

planarity (Supporting Information, Figure S2), as commonly found in crystal structures of substituted porphyrins as for example in the homo- and heterobimetallic ethene-linked bisporphyrins reported by Smith et al.[46] With respect to the PELDOR simulations, the most interesting feature is the intramolecular Cu^{2+}-nitroxide distance, which amounts to 21.254(3) and 20.185(3) Å for $Cu^{2+}-O$ and $Cu^{2+}-N$, respectively. Because the spin density is roughly equally distributed between the nitrogen and oxygen atom a mean distance of 20.7 Å can be extracted. The crystal structure also reveals that the porphyrin moieties stack onto each other, forming a nearly coplanar arrangement such that the next neighbour porphyrin ring is 3.621 Å apart (Supporting Information, Figure S2). This aggregation leads to the formation of "head-to-tail" structures with respect to the meso-substituent, where the unsubstituted meso-C(25) of one porphyrin is in close contact of 3.189 Å to the Cu^{2+} ion of the next porphyrin ring. The shortest intermolecular Cu−Cu distance amounts to 4.760 Å, whereas the next intermolecular Cu-(nitroxide-O) distance is 8.050 Å.[45] To avoid such intermolecular interactions, which have been reported for toluene solutions of Cu(OEP),[31a] 1-methylimidazole was added in excess to solutions used for PELDOR studies.[47]

PELDOR Measurements. A 2-pulse field swept spectrum of model compound **4** is depicted in Figure 3a. The PELDOR experiments were performed applying the pump pulse on the central line of the nitroxide (position A), to achieve large modulation depths, whereas the detection pulses were applied at higher frequency (positions B and C), to solely select spectral contributions from the copper(II) ion. The PELDOR time-trace recorded at detection position B (corresponding to a $\Delta\nu_{AB}$ of 226 MHz) is depicted in Figure 3b together with the time trace of a reference sample composed of an equimolar mixture of **1** and Cu(OEP). The PELDOR time trace of **4** exhibits three clearly resolved periods of modulation, whereas the reference measurement does not, proving that the modulation is only caused by intramolecular spin−spin coupling and not arising from intermolecular interactions or experimental artifacts.

The modulation depth λ of 0.40 is comparable to those found in time traces of bis-nitroxide systems using identical conditions for the pump pulse.[27] However, the damping of the modulation is much faster compared to structurally analogous bis-nitroxide model compounds (see Supporting Information),[17a,48] which can be due to different reasons. First, the spin density distribution in the porphyrin moiety might lead to a pronounced rhombicity in the spin−spin interaction. Second, the spectral selection on copper might correspond to a selection of distance vector orientations that leads to rapidly interfering frequencies. Third, the *g*-anisotropy of the copper-spin might cause a significant orientation dependence of g_A in eq 3, which leads to a dependence of the coupling strength not only on the orientation

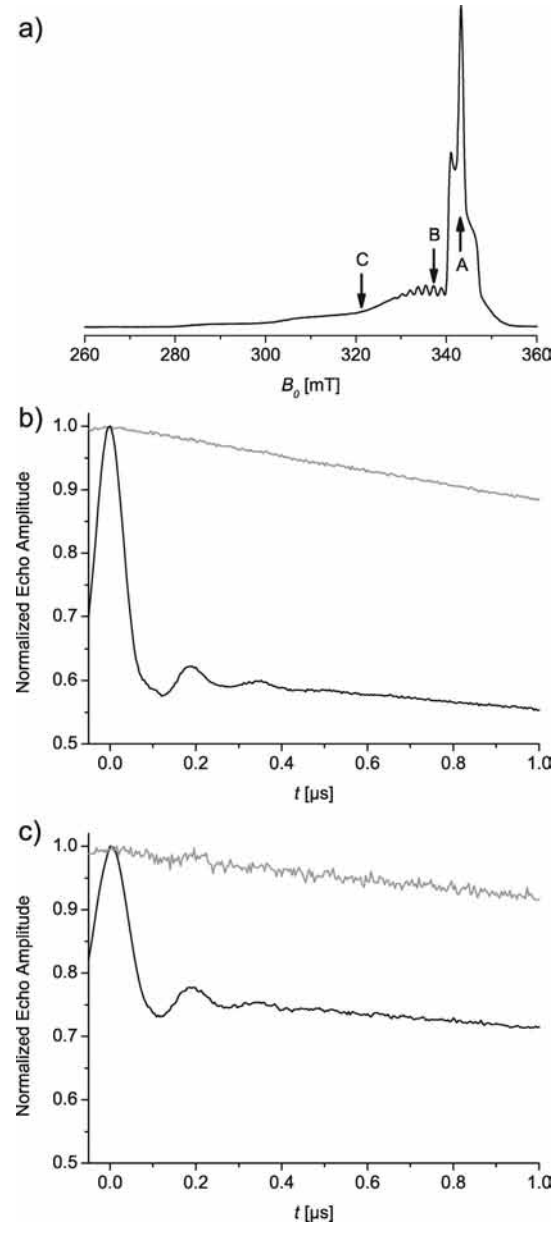

Figure 3. (a) Hahn-echo field swept spectrum of **4**. The following PELDOR experiments were performed with pumping at position A and detecting at B or C for a $\Delta\nu_{AB}$ of 226 or 603 MHz, respectively. (b) Experimental 4-Pulse PELDOR time trace of **4** with $\Delta\nu_{AB} = 226$ MHz (black line) together with a time trace recorded under the same conditions of a reference mixture of **1** and Cu(OEP) (1:1), shown in gray. (c) The 4-Pulse PELDOR time trace with $\Delta\nu_{AB} = 603$ MHz (black line) together with a time trace recorded under the same conditions of the same reference mixture, shown in gray.

of the distance vector but also on the orientation of the copper-porphyrin moiety with respect to the external magnetic field. Fourth, a high conformational flexibility of the porphyrin moiety. A high conformational flexibility of the biphenylene linker and the nitroxide spin-label in **4** is excluded, because this bridge is the same as in structural analogous bis-nitroxide systems. Fifth, an exchange coupling contribution *J*, which according to CW EPR data and simulations, is smaller than 0.2 MHz in average (see Supporting Information).

To investigate the effect of spectral selectivity on the PELDOR time traces, spectra of **4** were recorded with different frequency offsets $\Delta\nu_{AB}$; the one with the maximum offset of $\Delta\nu_{AB} = 603$ MHz (position C) is shown in Figure 3c, together

with the measurement on the reference sample under the same conditions.[49] The time trace shows three well-resolved modulation periods that are not present in the reference sample. Interestingly, slight changes in the shape of the modulation pattern, especially in the first minimum, can be seen compared to the measurement with $\Delta\nu_{AB} = 226$ MHz, indicating different orientation selections. The smaller λ of 0.23 compared to 0.40 at 226 MHz is due to the more selective π-pulse of 32 ns compared to the 12 ns pulse length used at 226 MHz. The reason for the longer pump pulse is the limited resonator bandwidth and thus the limited B_1 which does not allow shorter π-pulses at this large frequency offset. Time traces recorded with an offset of 226 MHz and 32 ns pump pulse length show similar modulation depths (see Supporting Information).

To investigate the influence of the spectral selection on the PELDOR spectra in more detail, the excitation efficiencies on the copper ion and on the nitroxide have been calculated for the pumping and detection frequencies corresponding to the frequency offsets $\Delta\nu_{AB} = 226$ MHz and $\Delta\nu_{AB} = 603$ MHz. The excitation profiles of the pulses were assumed to be Lorentizan. Figure 4 shows the resulting normalized excitation probabilities in dependence of the magnetic field orientation in the principle axis system of the respective molecule. Whereas all orientations of the nitroxide are pumped independent of the pump pulse length of either 12 or 32 ns, the selection on copper is more specific. Detecting at position B (corresponding to $\Delta\nu_{AB} = 226$ MHz), mainly Cu(OEP)-moieties with the molecular *x*- and *y*-axes (axes within the porphyrin plane) parallel to the magnetic field axis are selected, whereas those with the *z*-axis parallel to the field are not excited. In contrast, detecting at position C ($\Delta\nu_{AB} = 603$ MHz), the probability of Cu(OEP)-rings with the molecular *z*-axis parallel to the field increases, whereas *x* and *y* are deselected. Because the *g*-tensor is collinear to the molecular axis system, detecting at B mainly selects g_{xx} and g_{yy}, whereas detecting at C selects mainly noncanonical orientations.

To estimate the effect of the different selections on the PELDOR time-traces we calculated the form factors $P(\theta)$ (Figure 5), which describe within the point-dipole approximation the probabilities of excitation in dependence of the dipolar angle. The calculation has been performed by connecting the axis systems of the two spins and thus the two excitation profiles via the molecular structure, which is known from X-ray diffraction. To account for freezing-out a range of different conformations adopted by **4** at room temperature, a geometric/dynamic model was built taking into account the mean distance of 20.7 Å between the copper and the nitroxide, a single bending motion of 15° centered at the mid-point of the biphenyl bridge and free rotation of the nitroxide group around the phenolic bond on a cone of 31.4°. On the basis of this model, which has been proven to be useful for structurally analogous bis-nitroxides,[17] a conformational ensemble typically containing 1000 different conformers was generated. The form factors, calculated for these ensembles, show in either case significant deviation from the $\sin(\theta)$ probability distribution function of uncorrelated spin centers. For $\Delta\nu_{AB} = 226$ MHz, distance vectors parallel to B_0 ($\theta = 0°$) become more probable and those perpendicular to B_0 ($\theta = 90°$) less probable than expected for a $\sin(\theta)$ distribution. In case of $\Delta\nu_{AB} = 603$ MHz the intensities of both singularities are smaller than compared with the $\sin(\theta)$ function, whereas intermediate angles increase in probability. Thus, both form factors differ significantly from each other close to $\theta = 0°$. It is interesting to note that even though the form factors are quite different, this is not translated into a strong change in the experimental PELDOR time traces. It can, however, be visualized by Fourier transformation (see Supporting Information). The weak effect may be attributed to both

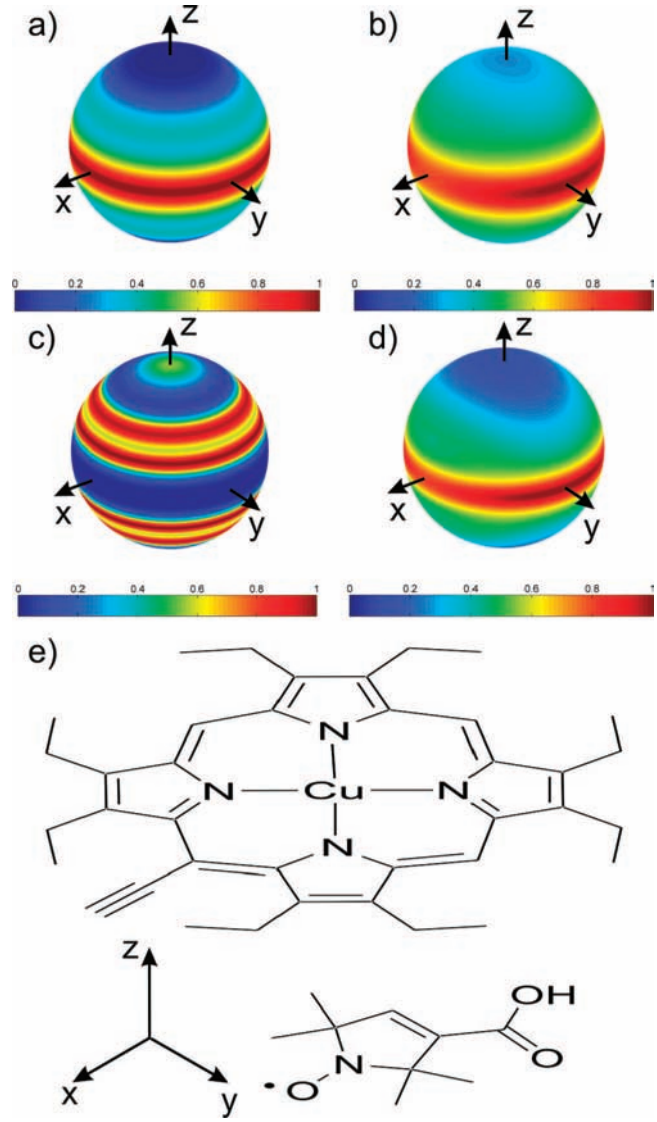

Figure 4. Orientation selection on copper with (a) $\Delta\nu_{AB} = 226$ MHz, $t_{PA} = 32$ ns and (c) $\Delta\nu_{AB} = 603$ MHz, $t_{PA} = 32$ ns. The orientation selection on the nitroxide is shown in (b) for $\Delta\nu_{AB} = 226$ MHz, $t_{PB} = 12$ ns and in (d) for $\Delta\nu_{AB} = 603$ MHz, $t_{PB} = 32$ ns. The molecular axis systems are depicted in (e).

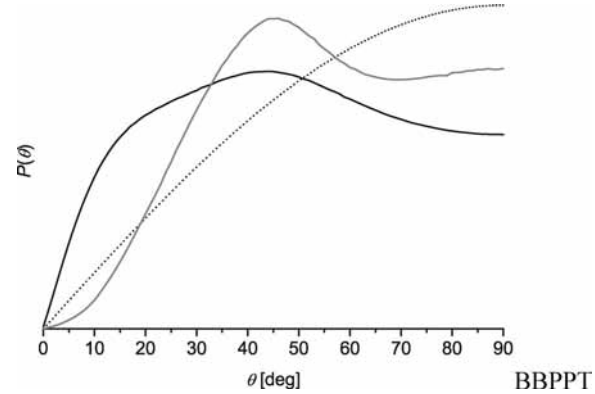

Figure 5. Calculated form factors $P(\theta)$ for the different frequency offsets of 226 MHz (black curve) and 603 MHz (gray curve). A $\sin(\theta)$ distribution for uncorrelated centers is shown for comparison (dotted line).

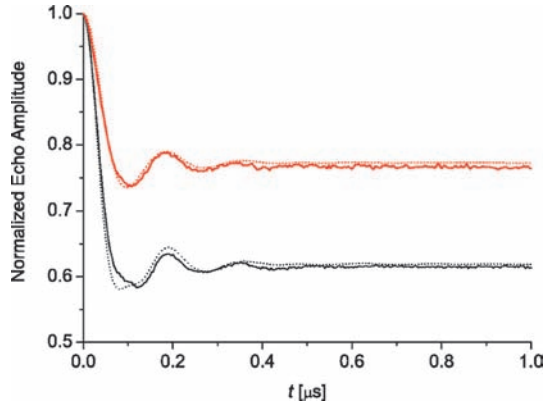

Figure 6. Simulations of the PELDOR time domain data of **4** assuming a Gaussian distribution of the copper nucleus in the porphyrin plane. The experimental time trace with $\Delta\nu_{AB} = 226$ MHz is shown in black and the one with $\Delta\nu_{AB} = 603$ MHz in red. Their simulations are overlaid as dotted lines.

form factors having maxima at approximately 45° and still strong intensity at $\theta = 90°$.

With the assumption that the damping is due to the flexibility of the copper atom in the porphyrin moiety, the time traces have been simulated employing the form factors as calculated above, and the explicit distance vector has been extracted from the geometric model. All calculated spectra are based on the identical geometric models and spin Hamiltonian parameters. Pulse lengths, frequencies, and magnetic field values were taken from the corresponding experiments. The flexibility of the copper was assumed to be described by a normal distribution in the porphyrin plane. If the width of this function was set to 1 Å (standard deviation) the simulation could be made to fit the experimental data (Figure 6). However, this flexibility model implies a large deformation of the porphyrin moiety with a standard deviation of ~30% of the porphyrin radius (3.5 Å). This and especially the implied significant elongation of the minimum energy structure is physically unreasonable.

Spin-density distribution in the Cu(OEP)-moiety may be an additional reason for the damping of the dipolar oscillation. To estimate the significance of the spin-density distribution, DFT calculations have been performed of the smaller but already asymmetric molecule **2** and Mulliken atomic spin densities have been computed. The resulting atomic spin densities are to 56% localized on the copper atom, 42% are equally distributed among the four nitrogen atoms (10.6% each), and 2% are delocalized within the rest of the porphyrin ring. (for details see Supporting Information). These values are in very good agreement with other calculations.[50] Experimental estimates from ENDOR data show slightly smaller spin densities on the porphyrin nitrogens (~8%).[51] Similar calculations for **1** show that its spin density is localized to 50% on the oxygen and to 45% on the nitrogen of the nitroxide group (Supporting Information).

To judge the effect the form factor has together with the spin density distribution on the PELDOR time traces, they have been simulated calculating the dipolar interaction tensor as specified in eq 8, but having the Cu nucleus fixed in the center of the porphyrin. Figure 7a demonstrates that despite the rather large spin density distribution, its effect on the simulated PELDOR time trace is only marginal.

On the other hand distortions of the porphyrin lead to different spin density distributions, especially the meso-carbon nuclei exhibit up to 5% spin density each in saddled porphyrins.[50] Possible asymmetric deformations were simulated by assigning 5% spin density on C_{meso}, 12% to the vicinal N, 9% to the

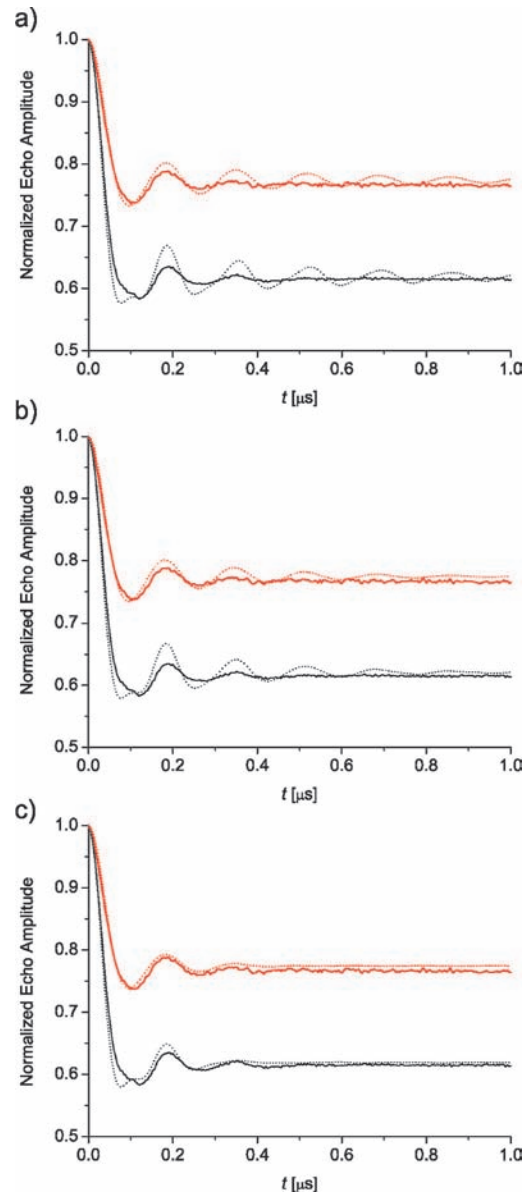

Figure 7. Simulations of the PELDOR time domain data of **4** treating the spin density distribution explicitly (a), assuming an ensemble of asymmetrically distorted porphyrins (b), and considering a distribution in exchange couplings of 0 ± 0.8 MHz (c). The experimental time trace with $\Delta\nu_{AB} = 226$ MHz is shown in black and the one with $\Delta\nu_{AB} = 603$ MHz in red. The respective simulations are overlaid as dotted lines.

remaining two N and 50% on copper. In addition, the copper nucleus was set 20 pm closer to C_{meso}. This polarization of the spin density leads to a slightly faster modulation period. Applying the inverse polarization and averaging those two signals to mimic an ensemble of asymmetrically distorted porphyrins leads to an increased damping but still does not reproduce the experiment (Figure 7b). Increasing the flexibility in the geometric model also leads to pronounced damping, but the conformational distributions needed to match the experiment contradict the findings on structurally analogous bis-nitroxides and make no physical sense (see Supporting Information).

However, the delocalization of spin density into the porphyrin-bridge system could lead to a small exchange coupling constant J[30,52] for which simulations of room temperature CW EPR spectra set an upper limit of ~0.2 MHz. Thus, freezing out a conformational ensemble might lead to a distribution in

exchange couplings, which is small on average. Good agreement of the data with the experiment was found for a normal distribution in J[53] centered at 0 with a standard deviation of 0.8 MHz (Figure 7c). In the case of the bisnitroxide systems, the localization of the spin density on the two NO groups and the two ester linkages prevent an exchange coupling. These simulations indicate that the damping of the modulation induced by the conformational flexibility alone is not sufficient to reproduce the experimentally observed damping, but that the time domain signal is a convolution of distributions in distances, spin densities, and exchange couplings induced by conformational heterogeneity. In addition, it is important to note, that not only the damping and modulation pattern is reproduced but that also the modulation depth is met for both pump pulse lengths (12 and 32 ns) using the same geometric model for both frequency offsets and thus indicating that the calculated form factors are reasonable.

Further simulations indicated that the shape of the first minimum depends strongly on mutual orientation of the spin-label with respect to the porphyrin ring (data not shown). Even though the assumption of full rotational freedom of the bridging acetylene and phenolic bonds works considerably well, deviations from this model may be the reason for the observed imperfection.

A convolution of the resonance frequencies of the two spins with the spin−spin coupling, to treat the different pulse selectivity in coupled systems, did not show significant effects on the simulations. Also the influences of the g-anisotropy of the Cu-center and from g-strains up to 1% on the dipolar coupling have been examined by simulations but were found to be negligible.

Finally, decreasing the frequency offset $\Delta\nu_{AB}$ in the simulations down to 100 MHz does not lead to a more pronounced appearance of the parallel component, as also observed experimentally (data not shown). The reason for the latter effect is probably due to "orientational smearing" caused by the isotropic nitrogen hyperfine coupling (~45 MHz). Thus, spectral selectivity on copper contributes to PELDOR at X-band but the effects are shallow.

Comparison with Data Inversion by Tikhonov Regularization. For the extraction of distance distributions ($P(r_{AB})$) in the limit of uncorrelated spin centers time domain data inversion by Tikhonov regularization based on eq 5 is the method of choice.[26] Even though this limit is not met in our case, the results of this method were investigated. Figure 8 shows the simulations based on the distance distributions obtained by inversion of both time traces of **4**. The main peak at 20.6 Å in both distance distributions matches nicely the distance inferred from the crystal structure and the fit of the time domain data is exceptional. However, additional distances appear at higher and smaller distance, which have no structural reasoning. The reason for these artifacts are the deviations of the form factors from sin θ, which is compensated by taking additional distances into account (the distance distribution is a best fit of $P(r_{AB})$ with $P(\theta) \sim \sin\theta$). When mutual orientations are fixed as in protein cofactors[11] and spectral selection is strong,[16] this approach, as implemented in recent PELDOR simulation programs, fails. Additionally, the width of these peaks is commonly interpreted to represent the conformational distribution of a biradical. Yet in the present case, this distribution does not represent the conformational flexibility of the molecule but a convolution of different spin delocalizations, a distribution in exchange couplings, and mobility. The simulating approach used here allows deconvoluting of the contributions and indeed, the width of

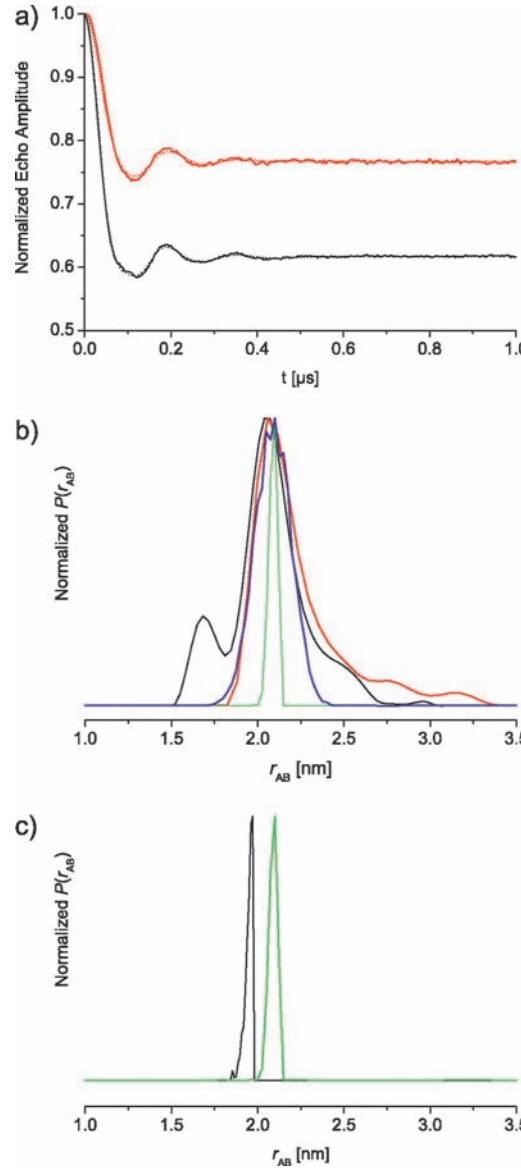

Figure 8. Results from Tikhonov regularizations: (a) experimental time traces with $\Delta\nu_{AB}$ = 226 MHz (black curve) and $\Delta\nu_{AB}$ = 603 MHz (red curve) and their simulations (dotted lines). In (b) the regularized distance distributions with $\Delta\nu_{AB}$ = 226 MHz (black curve) and with $\Delta\nu_{AB}$ = 603 MHz (red curve) are shown together with the distribution of spin−spin distances obtained from a Gaussian distribution of the Cu nucleus in the porphyrin plane (blue curve) and the distribution of copper-nitroxide distances from the same model without the Gaussian distribution (green curve). (c) Comparison of this narrow distance distribution (green) with the distance distribution obtained from data inversion on a structurally analogous bis-nitroxide (black).

$P(r_{AB})$ from the structural dynamics of the model (Figure 8b, green curve) is in good agreement with data from Tikhonov regularization obtained on a structurally analogous bis-nitroxide (Figure 8c and Supporting Information).

Conclusion

We showed on a newly synthesized, isolated, and fully characterized copper/nitroxide model system that orientation selectivity on copper effects PELDOR time traces at X-band frequencies although the experimentally observable differences are shallow. The chosen simulation approach also allowed for the deconvolution of effects contributing to the shape of PELDOR time traces: from the angular correlations the form

factors can be calculated disentangling distance distributions from spectral selectivity, spin density distribution, and exchange coupling. Thus, if the agreement between experimental data and simulation is good and if the experimental and spin Hamiltonian parameters are known, more information than mere distances can be extracted from PELDOR measurements, and structural models can easily be verified or disproved.

Acknowledgment. We thank Dr. Ute Bahr, J. W. Goethe-University, for recording mass spectra. This work has been supported by the Deutsche Forschungsgemeinschaft (SFB 579 ("RNA−ligand interactions") and the Center for Biomolecular Magnetic Resonance (BMRZ) Frankfurt. We gratefully acknowledge support by the Frankfurt Center for Scientific Computing. We thank Professor Dr. Gunnar Jeschke for helpful discussions.

Supporting Information Available: Synthesis of **2**, X-ray data, UV−vis and cw EPR spectra of **4** together with DFT calculations as well as further PELDOR data, further simulations, and Fourier transformations.

References and Notes

(1) (a) *Handbook of Metalloproteins*; Messerschmidt, A., Huber, R., Poulos, T., Wieghardt, K., Eds.; John Wiley & Sons, Ltd.: Chichester, England, 2001; Vol. 1, p 2. (b) DeGrado, W. F.; Summa, C. M.; Pavone, V.; Nastri, F.; Lombardi, A. *Ann. Rev. Biochem.* **1999**, *68*, 779.

(2) (a) Eckstein, F.; Lilley, D. M. J. *Nucleic Acids and Molecular Biology, Vol.* 10: *Catalytic RNA*; Springer: Berlin, 1995; (b) Gesteland, R. F.; Cech, T. R.; Atkins, J. F. *The RNA World*, 3rd ed.; Cold Spring Harbor: New York, 2006.

(3) (a) Fragai, M.; Luchinat, C.; Parigi, G. *Acc. Chem. Res.* **2006**, *39*, 909. (b) Arnesano, F.; Banci, L.; Piccioli, M. *Q. Rev. Biophys.* **2005**, *38*, 167–219.

(4) (a) Calle, C.; Sreekanth, A.; Fedin, M. V.; Forrer, J.; Garcia-Rubio, I.; Gromov, I. A.; Hinderberger, D.; Kasumaj, B.; Léger, P.; Mancosu, B.; Mitrikas, G.; Santangelo, M. G.; Stoll, S.; Schweiger, A.; Tschaggelar, R.; Harmer, J. *Helv. Chim. Acta* **2006**, *89*, 2495. (b) Bennati, M.; Prisner, T. F. *Rep. Prog. Phys.* **2005**, *68*, 411.

(5) (a) *Advanced EPR Applications in Biology and Biochemistry*; Hoff, A. J., Ed.; Elsevier: Amsterdam, 1989. (b) *Paramagnetic Resonance of Metallobiomolecules*; Telser, J., Ed.; ACS Symposium Series, Vol. 858; Oxford University Press: Oxford, 2003.

(6) (a) DeRose, V. *J. Chem. Biol.* **2002**, *9*, 961. (b) Kisseleva, N.; Kraut, S.; Jäschke, A.; Schiemann, O. *HFSP J.* **2007**, *1*, 127. (c) Kisseleva, N.; Khvorova, A.; Westhof, E.; Schiemann, O. *RNA* **2005**, *11*, 1. (d) Schiemann, O.; Fritscher, J.; Kisseleva, N.; Sigurdsson, S. T.; Prisner, T. F. *ChemBioChem* **2003**, *4*, 1057.

(7) Schiemann, O.; Prisner, T. F. *Q. Rev. Biophys.* **2007**, *40*, 1.

(8) (a) Voss, J.; Salwinski, L.; Kaback, H. R.; Hubbell, W. L. *Proc. Nat. Acad. Sci. U.S.A.* **1995**, *92*, 12295. (b) *Distance measurements in biological systems by EPR. Biological Magnetic Resonance*; Berliner, L. J., Eaton, S. S., Eaton, G. R., Eds.; Kluwer Academic/Plenum Publishers: New York, 2000; vol. 19.

(9) (a) Jeschke, G.;; Polyhach, Y. *Phys. Chem. Chem. Phys* **2007**, *9*, 1895. (b) Schiemann, O.; Piton, N.; Mu, Y.; Stock, G.; Engels, J. W.; Prisner, T. F. *J. Am. Chem. Soc.* **2004**, *126*, 5722.

(10) (a) Hara, H.; Kawamori, A.; Astashkin, A. V.; Ono, T.-a. *Biochim. Biophys. Acta* **1996**, *1276*, 140. (b) Elsässer, C.; Brecht, M.; Bittl, R. *J. Am. Chem. Soc.* **2002**, *124*, 12606. (c) Astashkin, A. V.; Seravalli, J.; Mansoorabadi, S. O.; Reed, G. H.; Ragsdale, S. W. *J. Am. Chem. Soc* **2006**, *128*, 3888.

(11) (a) Bennati, M.; Robblee, J. H.; Mugnaini, V.; Stubbe, J.; Freed, J. H.; Borbat, P. *J. Am. Chem. Soc.* **2005**, *127*, 15014. (b) Kay, C. W. M.; Elsässer, C.; Bittl, R.; Farell, S. R.; Thorpe, C. *J. Am. Chem. Soc.* **2006**, *128*, 76.

(12) (a) Milov, A. D.; Salikov, K. M.; Shirov, M. D. *Fiz. Tverd. Tela* **1981**, *23*, 975. (b) Larsen, R. G.; Singel, D. J. *J. Chem. Phys.* **1993**, *98*, 5134.

(13) (a) Borbat, P. P.; Freed, J. H. *Chem. Phys. Lett.* **1999**, *313*, 145. (b) Becker, J. S.; Saxena, S. *Chem. Phys. Lett.* **2005**, *414*, 248.

(14) Narr, E.; Godt, A.; Jeschke, G. *Angew. Chem., Int. Ed.* **2002**, *41*, 3907.

(15) (a) Amsterdam, I. M. C. v.;,; Ubbink, M.; Canters, G. W.; Huber, M. *Angew. Chem., Int. Ed.* **2003**, *42*, 62. (b) Kay, C. W. M.; Mkami, H. E.; Cammack, R.; Evans, R. W. *J. Am. Chem. Soc.* **2007**, *129*, 4868. (c) Yang, Z.; Becker, J.; Saxena, S. *J. Magn. Reson.* **2007**, *188*, 337.

(16) (a) Denysenkov, V. P.; Prisner, T. F.; Stubbe, J.; Bennati, M. *Proc. Natl. Acad. Sci. U.S.A.* **2006**, *103*, 13386. (b) Polyhach, Y.; Godt, A.; Bauer, C.; Jeschke, G. *J. Magn. Reson.* **2007**, *185*, 118. (c) Savitsky, A.; Dubinskii, A. A.; Flores, M.; Lubitz, W.; Möbius, K. *J. Phys. Chem. B* **2007**, *111*, 6245.

(17) (a) Godt, A.; Schulte, M.; Zimmermann, H.; Jeschke, G. *Angew. Chem., Int. Ed.* **2006**, *45*, 7560. (b) Margraf, D.; Bode, B. E.; Marko, A.; Schiemann, O.; Prisner, T. F. *Mol. Phys.* **2007**, *105*, 2153.

(18) (a) Kálai, T.; Balog, M.; Jekö, J.; Hideg, K. *Synthesis* **1999**, 973. (b) Schiemann, O.; Piton, N.; Plackmeyer, J.; Bode, B. E.; Prisner, T. F.; Engels, J. W. *Nat. Protoc.* **2007**, *2*, 904.

(19) Farrugia, L. J. *J Appl. Cryst.* **1999**, *32*, 837.

(20) Adler, A. D.; Longo, F. R.; Kampas, F.; Kim, J. J. *Inorg. Nucl. Chem.* **1970**, *32*, 2443.

(21) (a) Arnold, D. P.; Nitschinsk, L. J. *Tetrahedron* **1992**, *48*, 8781. (b) Inhoffen, H. H.; Fuhrhop, J.-H.; Voigt, H.; Brockmann, H. *Justus Liebigs Ann. Chem.* **1966**, *695*, 133. (c) Johnson, A. W.; Oldfield, D. *J. Chem. Soc. C* **1966**, 794. (d) Watanabe, E.; Nishimura, S.; Ogoshi, H.; Yoshida, Z. *Tetrahedron* **1975**, *31*, 1385. (e) Yeh, C.-Y.; Miller, S. E.; Carpenter, S. D.; Nocera, D. G. *Inorg. Chem.* **2001**, *40*, 3643.

(22) Hayashi, N.; Murayama, M.; Mori, K.; Matsuda, A.; Chikamatsu, E.; Tani, K.; Miyabayashi, K.; Miyake, M.; Higuchi, H. *Tetrahedron* **2004**, *60*, 6363.

(23) (a) Arnold, D. P.; James, D. A. *J. Org. Chem.* **1997**, *62*, 3460. (b) Arnold, D. P.; Hartnell, R. D. *Tetrahedron* **2001**, *57*, 1335.

(24) Mims, W. B. In *Electron Paramagnetic Resonance*; Geschwind, S., Ed.; Plenum: New York, 1972; pp 263.

(25) Milov, A. D.; Maryasov, A. G.; Tsvetkov, Y. D. *Appl. Magn. Reson.* **1998**, *15*, 107.

(26) (a) Jeschke, G.; Panek, G.; Godt, A.; Bender, A.; Paulsen, H. *Appl. Magn. Reson.* **2004**, *26*, 223. (b) Bowman, M. K.; Maryasov, A. G.; Kim, N.; DeRose, V. J. *Appl. Magn. Reson* **2004**, *26*, 23. (c) Chiang, Y.-W.; Borbat, P. P.; Freed, J. H. J. *Magn. Reson.* **2005**, *172*, 279.

(27) Bode, B. E.; Margraf, D.; Plackmeyer, J.; Dürner, G.; Prisner, T. F.; Schiemann, O. *J. Am. Chem. Soc.* **2007**, *129*, 6736.

(28) Mansoorabadi, S. O.; Reed, G. H. In *Paramagnetic Resonance of Metallobiomolecules*; Telser, J.,. Ed.; American Chemical Society: Washington, DC, 2003; pp 82.

(29) Cunningham, K. L.; McNett, K. M.; Pierce, R. A.; Davis, K. A.; Harris, H. H.; Falck, D. M.; McMillin, D. R. *Inorg. Chem.* **1997**, *36*, 608.

(30) Fritscher, J.; Beyer, M.; Schiemann, O. *Chem. Phys. Lett.* **2002**, *364*, 393.

(31) (a) Chikira, M.; Kon, H.; Hawley, R. A.; Smith, K. M. *J. Chem. Soc., Dalton Trans* **1979**, 245. (b) Iwaizumi, M.; Ohba, Y.; Iida, H.; Hirayama, M. *Inorg. Chim. Acta* **1984**, *82*, 47.

(32) Jeschke, G.; Chechik, V.; Ionita, P.; Godt, A.; Zimmermann, H.; Banham, J.; Timmel, C. R.; Hilger, D.; Jung, H. *Appl. Mag. Reson.* **2006**, *30*, 473.

(33) Jeschke, G.; Bender, A.; Paulsen, H.; Zimmermann, H.; Godt, A. *J. Magn. Reson.* **2004**, *169*, 1.

(34) Kohn, W.; Sham, L. J. *Phys. Rev.* **1965**, *140*, A1133.

(35) Ahlrichs, R.; Bär, M.; Baron, H.-P.; Bauernschmitt, R.; Böcker, S.; Crawford, N.; Deglmann, P.; Ehrig, M.; Eichkorn, K.; Elliott, S.; Furche, F.; Haase, F.; Häser, M.; Hättig, C.; Hellweg, A.; Horn, H.; Huber, C.; Huniar, U.; Kattannek, M.; Köhn, A.; Kölmel, C.; Kollwitz, M.; May, K.; Nava, P.; Ochsenfeld, C.; Öhm, H.; Patzelt, H.; Rappoport, D.; Rubner, O.; Schäfer, A.; Schneider, U.; Sierka, M.; Treutler, O.; Unterreiner, B.; Arnim, M. v.; Weigend, F.; Weis, P.; Weiss, H. *TURBOMOLE*, version 5.6; Quantum Chemistry Group, University of Karlsruhe: Karlsruhe, Germany, 2002.

(36) Frisch, M. J.; Trucks, G. W.; Schlegel, H. B.; Scuseria, G. E.; Robb, M. A.; Cheeseman, J. R. Montgomery, J.; Vreven, T.; Kudin, K. N.; Burant, J. C.; Millam, J. M.; Iyengar, S. S.; Tomasi, J.; Barone, V.; Mennucci, B.; Cossi, M.; Scalmani, G.; Rega, N.; Petersson, G. A.; Nakatsuji, H.; Hada, M.; Ehara, M.; Toyota, K.; Fukuda, R.; Hasegawa, J.; Ishida, M.; Nakajima, T.; Honda, Y.; Kitao, O.; Nakai, H.; Klene, M.; Li, X.; Knox, J. E.; Hratchian, H. P.; Cross, J. B.; Bakken, V.; Adamo, C.; Jaramillo, J.; Gomperts, R.; Stratmann, R. E.; Yazyev, O.; Austin, A. J.; Cammi, R.; Pomelli, C.; Ochterski, J. W.; Ayala, P. Y.; Morokuma, K.; Voth, G. A.; Salvador, P.; Dannenberg, J. J.; Zakrzewski, V. G.; Dapprich, S.; Daniels, A. D.; Strain, M. C.; Farkas, O.; Malick, K.; Rabuck, A. D.; Raghavachari, K.; Foresman, J. B.; Ortiz, J. V.; Cui, Q.; Baboul, A. G.; Clifford, S.; Cioslowski, J.; Stefanov, B. B.; Liu, G.; Liashenko, A.; Piskorz, P.; Komaromi, I.; Martin, R. L.; Fox, D. J.; Keith, T.; Al-Laham, M. A.; Peng, C. Y.; Nanayakkara, A.; Challacombe, M.; Gill, P. M. W.; Johnson, B.; Chen, W.; Wong, M. W.; Gonzalez, C.; Pople, J. A. *Gaussian 03*, revision C.02; Gaussian Inc: Pittsburgh, PA, 2004.

(37) Becke, A. D. *Phys. Rev. A* **1988**, *38*, 3098.

(38) (a) Perdew, J. P. *Phys. Rev. B* **1986**, *33*, 8822. (b) Perdew, J. P. *Phys. Rev. B* **1986**, *34*, 7406.

(39) Schafer, A.; Huber, C.; Ahlrichs, R. *J. Chem. Phys.* **1994**, *100*, 5829.

(40) (a) Eichkorn, K.; Treutler, O.; Öhm, H.; Haser, M.; Ahlrichs, R. *Chem. Phys. Lett.* **1995**, *242*, 652. (b) Eichkorn, K.; Weigend, F.; Treutler, O.; Ahlrichs, R. *Theor. Chem. Acc* **1997**, *97*, 119.

(41) Becke, A. D. *J. Chem. Phys.* **1993**, *98*, 5648.

(42) (a) Perdew, J. P.; Wang, Y. *Phys. Rev. B* **1992**, *45*, 13244. (b) Perdew, J. P. *Physica B* **1992**, *172*, 1.

(43) Arbuznikov, A. V.; Vaara, J.; Kaupp, M. *J. Chem. Phys.* **2004**, *120*, 2127.

(44) Kutzelnigg, W.; Fleischer, U.; Schindler, M. In *NMR Basic Principles and Progress*; Diehl, P., Fluck, E., Günther, H., Kosferld, R., Seelig, J., Eds.;Springer-Verlag: Berlin/Heidelberg, Germany, 1990; Vol. 23, p 165–262.

(45) Bolte, M.; Plackmeyer, J. *Acta Cryst.* **2006**, *E62*, e22.

(46) (a) Senge, M. O.; Vicente, M. G. H.; Gerzevske, K. R.; Forsyth, T. P.; Smith, K. M. *Inorg. Chem.* **1994**, *33*, 5625. (b) Clement, T. E.; Nurco, D. J.; Smith, K. M. *Inorg. Chem.* **1998**, *37*, 1150.

(47) CW X-band EPR studies of **4** without 1-methylimidazole showed strong half-field signals at $g = 4$ indicative of close spin−spin contacts. These signals disappeared completely upon adding 1-methylimidazole.

(48) Weber, A.; Schiemann, O.; Bode, B.; Prisner, T. F. *J. Magn. Reson.* **2002**, *157*, 277.

(49) Offsets larger than 603 MHz are not feasible due to limited B_1 and signal-to-noise ratio.

(50) Shao, J.; Steene, E.; Hoffman, B. M.; Ghosh, A. *Eur. J. Inorg. Chem.* **2005**, *2005*, 1609.

(51) (a) Iwaizumi, M.; Kudo, T.; Kita, S. *Inorg. Chem.* **1986**, *25*, 1546. (b) Astashkin, A. V.; Raitsimring, A. M.; Walker, F. A.; Rensing, C.; McEvoy, M. M. *J. Biol. Inorg. Chem.* **2005**, *10*, 221.

(52) Elschenbroich, C.; Wolf, M.; Schiemann, O.; Harms, K.; Burghaus, O.; Pebler, J. *Organometallics* **2002**, *21*, 5810.

(53) In case of a small exchange coupling, the spin−spin coupling ω_{AB} is defined as $\omega_{dd} + J$ with the exchange coupling Hamiltonian given by $\hat{H}_J = J\,\hat{S}_A\hat{S}_B$.

JP710504K